Ore Geology Reviews 86 (2017) 212–224

Contents lists available at ScienceDirect

Ore Geology Reviews

journal homepage: www.elsevier.com/locate/oregeo

Structural control on overprinting high-sulfidation epithermal on porphyry mineralization in the Chodarchay deposit, northwestern Iran

Narges Yasami [a], Majid Ghaderi [a,*], Saeed Madanipour [a], Behzad Taghilou [b]

[a] Department of Geology, Tarbiat Modares University, Tehran 14115-175, Iran
[b] Department of Environmental Sciences, University of Zanjan, Zanjan, Iran

ARTICLE INFO

Article history:
Received 24 August 2016
Received in revised form 20 December 2016
Accepted 30 January 2017
Available online 12 February 2017

Keywords:
Remote sensing
Structural control
Overprinting
Chodarchay deposit
Tarom
Iran

ABSTRACT

The Chodarchay high-sulfidation epithermal-porphyry deposit is located in the Tarom volcano-plutonic subzone of Western Alborz structural zone in NW Iran. In addition to Chodarchay, the Tarom subzone hosts several other epithermal deposits. Lithologic units in Chodarchay consist of volcanic-pyroclastic rocks and intrusive bodies. Petrographical studies have identified different rocks which host the mineralization. Mineralization has taken place in both volcanic-pyroclastic units and intrusions. Detailed mineralogical and alteration data gathered from drill cores and thin sections provides support for the hypothesis that the high-sulfidation epithermal mineralization is underlain by a porphyry copper system. This deposit is the first reported porphyry-epithermal mineralization in this subzone. The main structure of the Chodarchay area is a fault zone that formed parallel to the general Tarom NW-SE direction. Based on remote sensing studies, on a wider scale, lineaments generally show NE-SW trends, but the Chodarchay fault zone has a NW-SE strike and is associated with another W-E trending fault zone. These fault zones are correlated with argillic alteration. There are two sets of reverse fault fractures with a strike-slip component, based on slickenlines in the field and core observations. A normal sense of fault movement remains in the NW part of the structural system. These new data sets indicate two main extensional and compressional mechanisms for the fault. The evolution of the fault system from normal to reverse in the deposit characterizes the present day structural system of the Chodarchay area. Plutonism and porphyry mineralization are related to the extensional stage, whereas the epithermal part of the deposit is associated with the compressional stage of fault activation.

1. Introduction

Porphyry copper deposits are formed by hydrothermal fluids separated out from solutions from subduction-related arc magmatism (e.g., Richards, 2005). The magmatic arc region of a subduction zone could experience different tectonic regimes from extension to compression. In magmatic arcs, where the subducting and overriding plates obliquely converge, transpression or transtension tectonic regime is dominant (e.g., Uyeda, 1982; Taylor and Martinez, 2003; Heuret and Lallemand, 2005; Heuret et al., 2007). The anatomy of porphyry deposits at convergent margin tectonic settings with compressional to extensional states was outlined by Tosdal and Richards (2001). The transpression tectonic in the back-arc region could cause local relaxation of compressive stress in the fault jogs that may produce extensional areas providing an efficient locus for magma ascent and porphyry copper mineralization (e.g., Berger and Drew, 1997; Berger et al., 1999; Drew et al., 1999a,b; Drew and Berger, 2001, 2002; Tosdal and Richards, 2001; Carranza and Hale, 2002). Inversion of major faults from normal to thrust is one of the most prominent structural features in the back-arc regions that experienced transpression tectonics. The reactivation of the faults could lead to overprinting of a different mineralization system to existing porphyry deposits in the back-arc region (e.g., Berger and Drew, 1997; Berger et al., 1999).

Tarom subzone of the Alborz magmatic belt is formed in the back-arc region of the Neo-Tethyan subduction zone. The belt was initially formed in an extensional tectonic setting during Late Paleocene - Eocene (e.g., Vincent et al., 2005; Verdel et al., 2011). Early Oligocene compressional deformation related to the initial collision of the Arabia and Eurasia plates inverted the extensional structures of the Alborz magmatic belt (e.g., Allen et al., 2003; Guest et al., 2007; Madanipour et al., 2013). This structural inversion could have affected the spatial and temporal distribution of the ore deposits across the belt. It might have also caused over-

* Corresponding author.
E-mail address: mghaderi@modares.ac.ir (M. Ghaderi).

http://dx.doi.org/10.1016/j.oregeorev.2017.01.028
0169-1368/

printing of different mineralization systems on early porphyry deposits which formed during Early Paleocene - Eocene arc-related magmatism. The spatial and temporal relation between structural inversion and different ore mineralization systems is poorly studied in the Tarom subzone of the Alborz magmatic belt. The Chodarchay copper deposit in the Tarom subzone could provide a very good case of structural control on this type of overprinting (Fig. 1a-b). The overprinting of epithermal mineralization on porphyry mineralization in Chodarchay deposit combined with the structural data which present both extensional and compressional features makes it a unique area for studying the effect of inversion tectonics on mineralization overprinting process.

Previous studies in the Tarom subzone focused only on occurrence of mineralization such as interpretation of lineament tectonics, the relation between Cu mineralization and major faults with no attention to mineralization overprinting (Aghazadeh et al.,

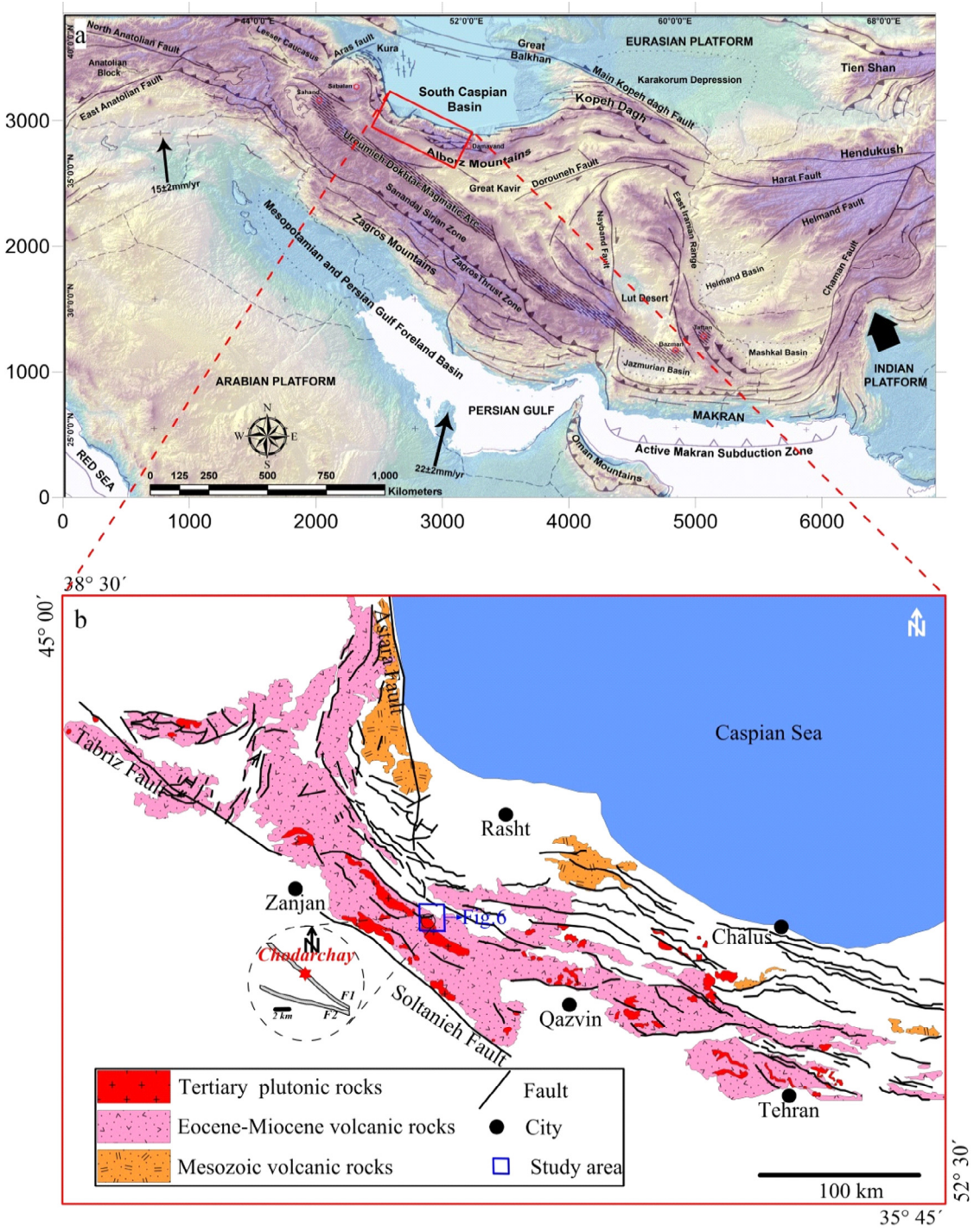

Fig. 1. a) General structural features in the Arabia-Eurasia continental collision zone. The brown shaded areas represent the highly elevated regions of the Arabia-Eurasia collision zone. The GPS velocity vectors (black arrows in mm/year) show the velocity of the Arabian Plate relative to the fixed Eurasia Plate (Vernant et al., 2004). Red rectangle represents the location of Fig. 1b. b) Structural geology map of the northwestern part of the Iranian Plateau. Tertiary volcanic rocks and intrusive bodies mark the location of the Alborz magmatic belt and Tarom subzone. Structural trends of the area are generally NW-SE. Structural elements of the Chodarchay ore deposit including the F1 and F2 faults are presented in an inset circle. (For interpretation of the references to color in this figure legend, the reader is referred to the web version of this article.)

2011; Nouri et al., 2013; Nabatian et al., 2014, 2016; Arian and Nouri, 2015). In this study, efforts have been made to elaborate in more detail on how structural features could be responsible in formation of a system comprising both porphyry and epithermal mineralization. Structural and mineralogical analysis on major controlling faults represent the overprinting of epithermal mineralization on an earlier porphyry deposit in the Tarom subzone of the Alborz magmatic belt. The overprinting of epithermal mineralization on the porphyry deposit occurred due to the inversion of major faults from normal kinematics to reverse movements.

2. Geological setting of Chodarchay

The Iranian Plateau has experienced a complex set of deformation, volcanism and magmatism at the northwestern margin of the Arabia-Eurasia collision zone during the Late Cenozoic. Paleocene-Eocene extensional tectonics and related volcanism in response to subduction and roll-back of the Neo-Tethys ocean is a major event recorded across the collision zone (e.g., Berberian and King, 1981; Vincent et al., 2005; Verdel et al., 2011). Late Eocene–early Oligocene is the timing of the initial collision between the Arabia and Eurasia plates (Agard et al., 2005; Vincent et al., 2005, 2007; Allen and Armstrong, 2008; Horton et al., 2008; Madanipour et al., 2013). The earlier deformation is mainly restricted to a very narrow belt between the Sanandaj-Sirjan zone and the High Zagros; however, the effects of the final collision between the Arabian and Eurasian plates have been recorded in the Zagros and Alborz Mountains during the middle Miocene (e.g., Allen et al., 2004; Agard et al., 2005; Guest et al., 2007; Fakhari et al., 2008). Subduction of Neo-Tethys oceanic crust beneath the Iranian plate, and following Arabia-Eurasia collision throughout the Alpine–Himalayan orogeny, caused the volcanism in the Sanandaj–Sirjan Zone, the Urumieh–Dokhtar Magmatic Arc, the Alborz Magmatic Belt and the Zagros fold-and-thrust belt (e.g., Stöcklin, 1974; Berberian and King, 1981) (Fig. 1a). The Sanandaj–Sirjan Zone is regarded as the main magmatic arc arising from Neo-Tethyan subduction during the Mesozoic (Azizi et al., 2011; Berberian and King, 1981), although the Urumieh–Dokhtar Magmatic Arc and the Alborz Magmatic Belt are attributed to early to late Cenozoic subduction-related magmatism in the Zagros hinterland (Berberian and King, 1981; Berberian et al., 1982; Stöcklin, 1971), slab break-off (Agard et al., 2011; Ghasemi and Talbot, 2006; Haschke et al., 2010), slab roll-back (Jahangiri, 2007; Verdel et al., 2011) and post-collisional relaxation (Castro et al., 2013; Nabatian et al., 2014). Various petrogenetic models, such as continental arc magmatism (Berberian and Berberian, 1981; Hassanzadeh, 1993), continental rifting (Amidi et al., 1984), and post-collisional tectonic setting (Aghazadeh et al., 2011; Ahmadian et al., 2009; Berberian and King, 1981; Castro et al., 2013; Honarmand et al., 2013; Nabatian et al., 2014), have been suggested for some of the magmatic segments in the Urumieh–Dokhtar Magmatic Arc and the Alborz Magmatic Belt.

The Chodarchay deposit is located east of Zanjan, in the Tarom volcano-plutonic belt which is part of the Alborz Magmatic Belt. This belt formed as a result of the Western Alborz Tertiary magmatism with a NW-SE strike. The Western Alborz is part of the Eurasia metallogenic belt (Fig. 1a-b) (Janković, 1977). Paleocene to Miocene volcanics, volcaniclastics and intrusive bodies are the main rock units in the Tarom Mountains, which have been affected by general folding and faulting during the late Cenozoic. Most of the volcanic and volcaniclastic rocks in the district have traditionally been assigned to the Karaj Formation (Hirayama et al., 1966), although some rocks were correlated with Oligocene units. Trachyte, trachy-andesite, andesite, basaltic andesite, olivine–basalt and rhyodacite with Eocene ages and high-K calc-alkaline to alkaline magmatic affinities are the most common lava and pyroclastic rock units in the marine volcanism (Asiabanha and Foden, 2012; Moayyed, 2001; Nabatian et al., 2014). These lithologic units are potassic and have a shoshonitic nature (Asiabanha and Foden, 2012; Moinvaziri, 1985). Units at the base of the Karaj Formation have U-Pb zircon ages of 49.3 ± 2.9 Ma to 41.1 ± 1.6 Ma age (Verdel et al., 2011). Linear plutons in the Tarom belt had been emplaced at shallow depths during the late Eocene to early Oligocene (Castro et al., 2013; Nabatian et al., 2016).

The Karaj Formation in the central and western Alborz is part of the Eocene Alborz magmatic assemblage deposited within an arc and back-arc tectonic setting in an extensional regime in a post-collisional environment (Allen et al., 2003; Asiabanha and Foden, 2012; Ballato et al., 2011; Berberian, 1983; Hassanzadeh et al., 2002; Mirnejad et al., 2010). Nabatian et al. (2016) argued that an extensional tectonic regime has been dominant during the late Eocene in the Tarom region. Several processes and reasons have been suggested for this extensional tectonic regime during the late Eocene such as slab roll-back (Verdel et al., 2011), progressive linkage of the two plates and subtractive subduction (Agard et al., 2011), back-arc setting (Asiabanha and Foden, 2012) and post-collisional uplift (Asiabanha and Foden, 2012; Castro et al., 2013; Karsli et al., 2007; Nabatian et al., 2014). The extension would allow asthenospheric upwelling and partial melting of the metasomatized mantle to produce K-rich intrusions in the Tarom region. Variable degrees of partial melting of the metasomatized mantle source have occurred due to their chemical compositional variations and P–T conditions, before decompression (Nabatian et al., 2016).

The kinematics of the major faults in NW of the Alborz belt are generally thrust movements with a right to left lateral strike slip component (Fig. 1b). There are also some faults with pure thrust or strike slip kinematics that represent the partitioning effect of the deformation related to collisional process in this part of the Arabia-Eurasia collision zone (e.g., Jackson et al., 2002). Structural evidence from some of the faults in the belt, including the Masuleh Dagh Fault at southern border of the Talesh Mountains, indicate a major kinematic change from normal movement in the Paleocene-Eocene to thrust movement in the middle Miocene (Madanipour et al., 2013). Major faults in the Chodarchay deposit include faults F1 and F2. Their orientations are similar to other major structures in the Alborz magmatic belt and are NW-SE trending (Figs. 1b and 2). The F1 and F2 faults in accordance with deformation phases of Alborz magmatic belt demonstrate both extensional and compressional kinematic features.

Lithologic units in the Chodarchay deposit consist of lavas, pyroclastics and intrusions. Petrographic and geochemical evidence indicates that the plutons in the Tarom subzone are I-type granitoids (e.g., Nabatian et al., 2016). The oldest exposed rocks within the Chodarchay district consist of Karaj Formation units in most parts of the district (Fig. 2). The volcanic and pyroclastic rocks in the area were intruded by late-stage magmatic stocks. These consist of one broad suite of early quartz monzonite to quartz syenite porphyry and an alkali granite porphyry stock. Therefore, two discontinuous cycles of magmatic activities have been identified in the Chodarchay area. During the first cycle, volcanic and volcaniclastic units of the Karaj Formation erupted (Hirayama et al., 1966). Subvolcanic and plutonic bodies of quartz monzonite to quartz syenite and alkali granite were emplaced as small porphyries in the second cycle of magmatic activity. The Cu-Au Chodarchay deposit is hosted by a quartz monzonite to quartz syenite pluton and surrounding volcanic-volcaniclastic wall rock, such as rhyolitic lithic crystal tuff, rhyolite, andesite and breccias.

Mineralization at Chodarchay deposit consists of two types: 1-HS epithermal type and 2- porphyry type. The HS epithermal part of the deposit overprints the lower porphyry mineralization. The porphyry type mineralization does not contain economically

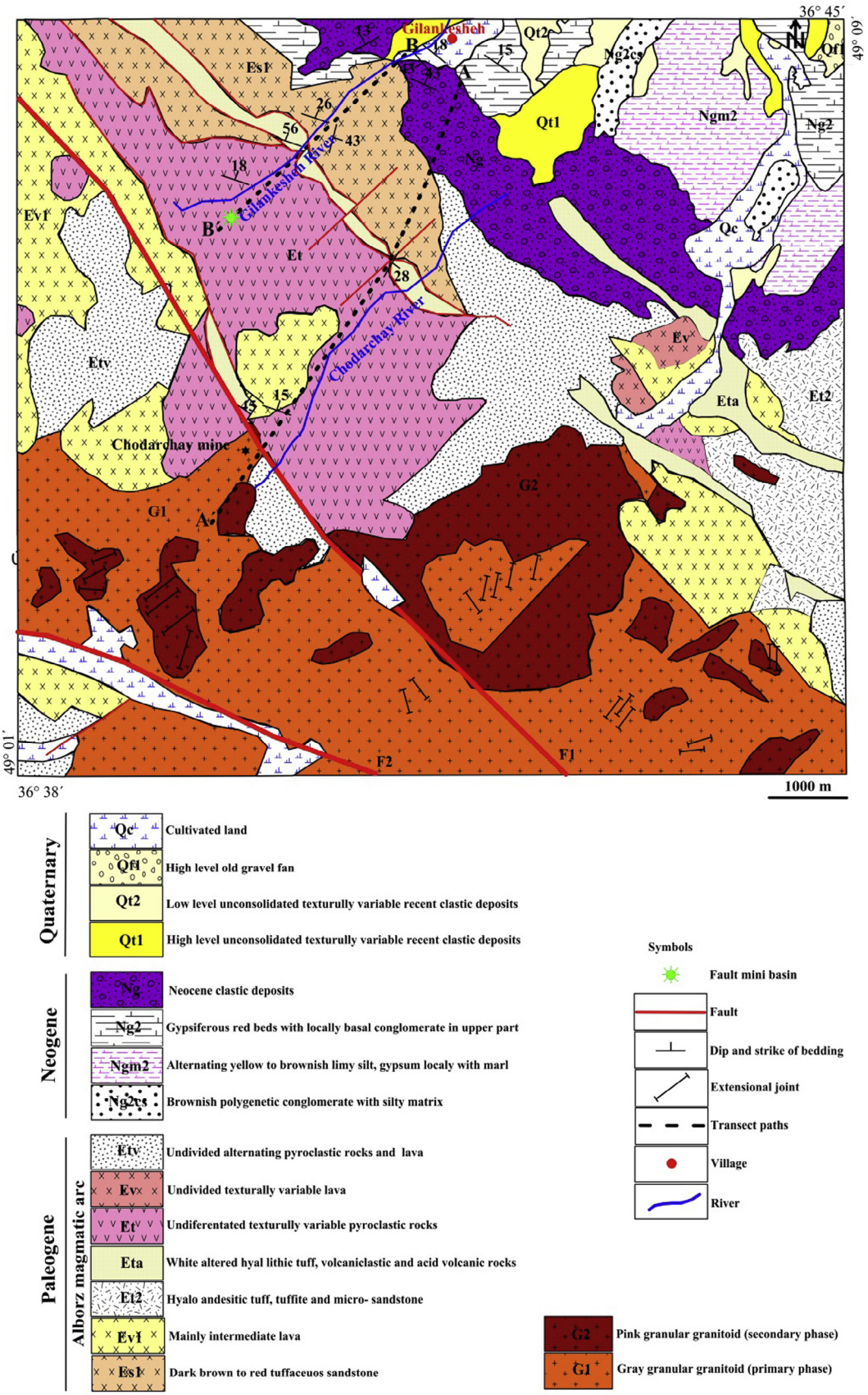

Fig. 2. Geological map of the study area revised and modified based on the new field data from 1:100,000 geological map of Roudbar (modified after Nazari and Salamati, 1998). Star marks the location of the Chodarchay deposit. The structural lines (AA′ and BB′) are shown by black dash-lines.

important quantities of ore, but as the Chodarchay deposit is the first porphyry deposit recognized in the Tarom subzone, it is important for exploration. Porphyry ore is found at deeper parts of the quartz-monzonite as disseminated Cu and Fe ores. It is overprinted by epithermal-type mineralization. The porphyry ore deposit has disseminated chalcopyrite and magnetite at deeper levels of the deposit in the potassic alteration zone. This is the first report and proof of a porphyry ore deposit in the Tarom subzone. Potassic alteration is especially common and important in porphyry and epithermal mineral systems, where it occurs in the high temperature core zones. K-feldspar and biotite are indicator minerals for potassic alteration in porphyry deposits.

3. Materials and methods

This study has been carried out to determine the structural and hydrothermal environment of the Chodarchay deposit by remote sensing techniques, field and subsurface analysis. Here, we combined satellite image processing including spectral and spatial enhancement, field geology, logging of drill cores, petrography-mineralography studies, and geological cross sections to reconstruct the structural and hydrothermal evolution of the deposit.

3.1. Image processing and remote sensing

Satellite images for mineral exploration have benefited geologists, scientists and exploration managers due to the sensor containing multiple band colors which allows them to interpret wavelengths that cannot be seen by the human eye, such as near infrared, short wave infrared and thermal infrared to identify the difference in structural features of the earth's surface. Process and interpretation of the these images are also the first step in recognizing and documenting fault zones and their related effect on other geological features including generation and distribution of the mineral resources. Several mineral deposits and fault systems have been documented in the Tarom subzone of the Alborz Magmatic belt. However the relationships between fault zones and distribution of the mineral deposits have not been investigated there. We have used satellite images to examine the structural and alteration features of the Tarom area. We also used the satellite images to acquire all different kinds of lineaments in study area. These lineaments generally include real fault zones, topographic and vegetation lines. However, we used field observations to distinguish between different kinds of lineaments and real fault zones.

Recorded Digital Numbers (DNs) in satellite data usually have low values and in black and white (gray) images they have values between 0 and 255. Therefore, details are not usually visible to the human eyes. For spectral enhancement, various techniques, such as band ratio false color combination, have been used for sharpening. Digital processing techniques have enhanced the quality of the images and include false color composites, ratio image of ETM+ 5, ETM+ 7 and the Sultan band ratio color composite image. These combinations allow us to perfectly distinguish the mineralization area at Chodarchay ore deposit region. These images were downloaded from on the Earth explorer site. Image p166R35 was selected and includes the study area. To reduce atmospheric effects, including scattering and absorption which cause haze and produce low contrast images (Richards and Xiuping, 2006), radiometric correction has been applied to the raw satellite data.

3.2. Structural analysis

3.2.1. Surface data processing

Structural geometry and distribution of rock units in the Chodarchay deposit area were characterized using a combination of bench and outcrop mapping and core logging in the field. Particular attention was given to contacts and cross-cutting relationships. Individual lithologies were examined in the outcrop, on polished slabs, and in thin sections. In order to identify the ore and gangue mineral assemblages and supergene minerals for the Chodarchay deposit, 72 thin-polished and 70 thin sections were prepared and examined by reflected light microscopy. Two structural cross sections were constructed to display lithologic and structural data obtained from the study area.

3.2.2. Subsurface or core data analysis

Several vertical boreholes have been drilled in the Chodarchay area to estimate the spatial distribution of the deposit. Valuable structural data, including orientations of fault and joint systems, have been documented in the drill core data set. We have measured the fracture angles with respect to core axes and then converted them to their actual dip angle with respect to the horizontal. 1204 discontinuities including faults and joints, 224 siliceous veinlets, 39 carbonated veinlets and 84 tourmaline veinlets have been measured in cores from the Chodarchay deposit. Statistical analysis has been performed on data sets gathered from drill core to document the major structural features in the Chodarchay deposit area.

4. Results

4.1. Characteristics of the Chodarchay Cu-Au porphyry-epithermal deposit

As revealed by ore microscopy studies, the Chodarchay porphyry-epithermal system contains chalcopyrite, pyrite, galena, sphalerite, enargite, tetrahedrite-tennantite, covellite, digenite, bornite and a few other minerals such as magnetite, hematite,

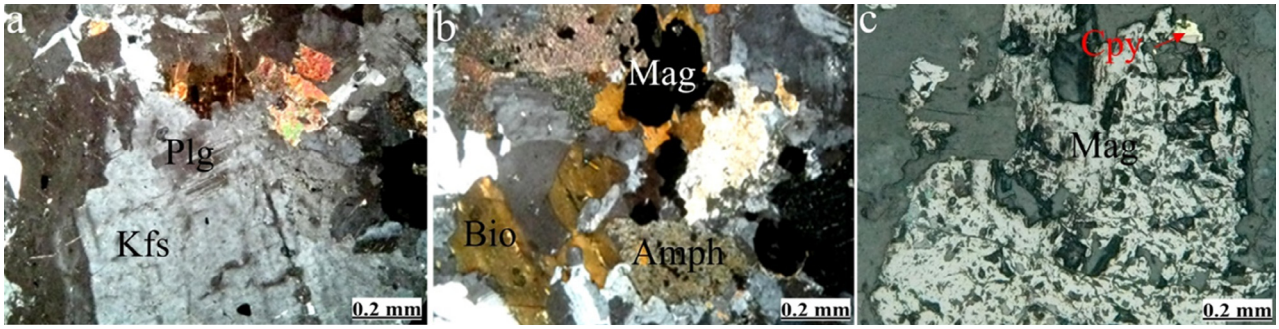

Fig. 3. Potassic alteration (secondary alkali feldspar, secondary biotite, magnetite and chalcopyrite) is associated with porphyry type mineralization: a) replacement of plagioclase by secondary alkali feldspar; b) amphibole converts into secondary biotite; c) disseminated magnetite and chalcopyrite in potassic altered parts of the Chodarchay deposit. Kfs: Alkali feldspar, Plg: Plagioclase, Mag: Magnetite, Bio: Biotite, Amph: Amphibole, Cpy: Chalcopyrite.

ilmenite, pyrolusite, rutile and gold. The tiny gold grains are in hydrothermal quartz. Later supergene oxidation of sulfide minerals led to deposition of secondary minerals such as malachite, azurite, turquoise and Fe oxides. Mineralization was multistage with different geometries including veinlets, open space filling, mineralized hydrothermal breccias and disseminated mineralization.

The underground alteration zones and ore bodies have similar orientations, and also have a similar orientation to the fault zone associated with the Chodarchay deposit, suggesting structural control. Alteration types in the study area consist of potassic, propylitic, sericitic, sericitic-tourmaline, argillic, advanced argillic and silicic.

The ore mineralogy of the Chodarchay epithermal-porphyry deposit was supplemented by field mapping and detailed microscopy studies. Mineralogy studies and petrographic examinations show that the deposit is associated with two distinct mineralization and alteration types (porphyry and HS type mineralization). Porphyry type mineralization is associated with potassic (K-feldspar + biotite + magnetite) alteration. Chalcopyrite is the predominant sulfide mineral found under microscope at the Chodarchay porphyry Cu deposit. Fine-grained chalcopyrite crystals are observed as disseminations in the host stock (Fig. 3a-c). Base metal sulfides and sulfosalts are the main ore minerals in the HS epither-

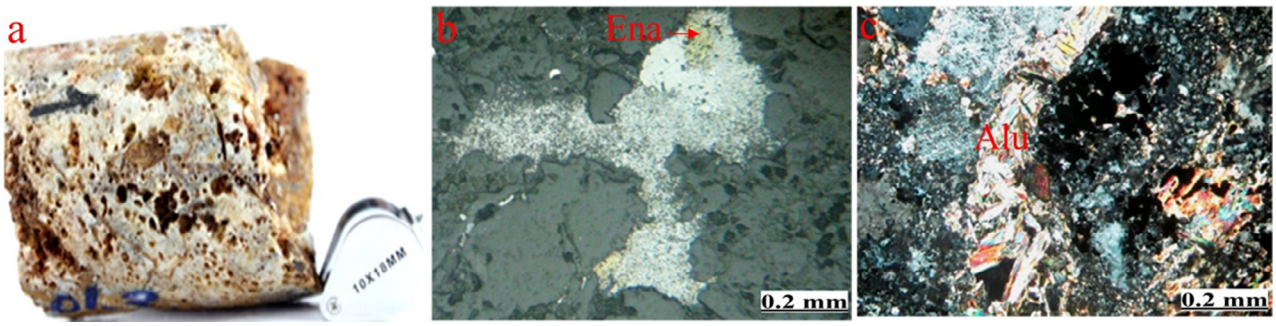

Fig. 4. Some observations on the Chodarchay deposit point out to high-sulfidation epithermal mineralization: a) vuggy quartz from hot acid fluid leaching; b) deposition of enargite occurs in high-sulfidation epithermal deposits; and c) presence of alunite indicates strongly acid fluid. Ena: Enargite, Alu: Alunite.

Table 1
Calculated statistical parameters of raw Landsat ETM+ data for Chodarchay area.

Scene	Stats	Min	Max	Mean	Stdev
P166 R 35	Band 1	0	255	48.80	34.26
	Band 2	0	255	50.55	36.36
	Band 3	0	255	66.86	49.28
	Band 4	0	255	58.14	42.06
	Band 5	0	255	66.08	48.72
	Band 6	0	255	54.16	40.57
	Band 7	0	255	60.16	43.46
Study area	Band 1	43	108	63.22	6.34
	Band 2	30	106	58.08	8.22
	Band 3	29	135	70.47	13.21
	Band 4	23	119	62.45	10.45
	Band 5	20	137	70.66	14.21
	Band 6	14	104	55.21	11.85
	Band 7	21	128	64.94	10.58

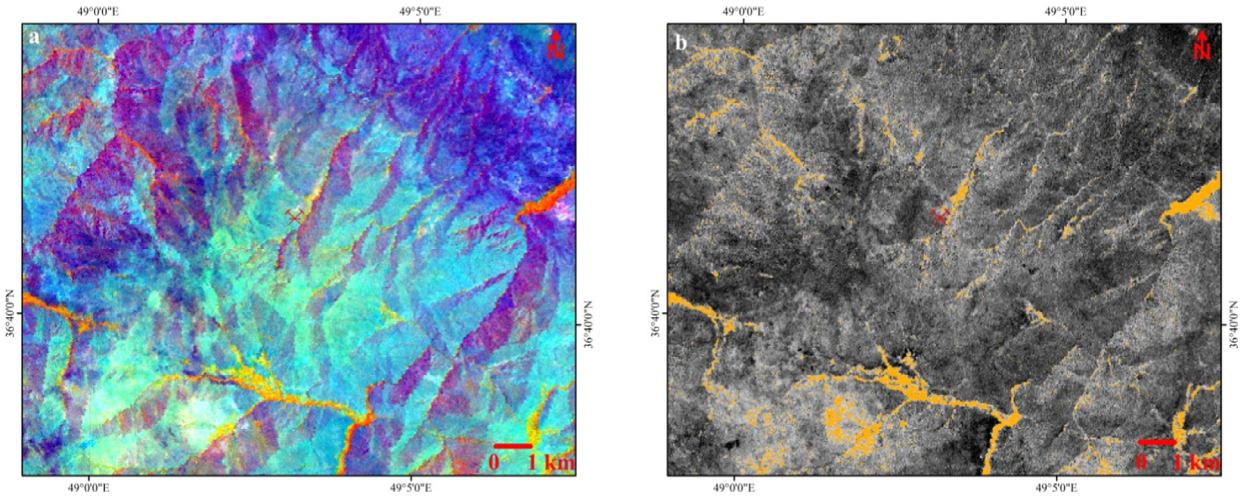

Fig. 5. a) Sultan's color composite ratio image of bands 5/7, 5/1 and (5/4 * 3/4) in RGB, respectively; b) ratio image of ETM+ 5/7.

mal part. Vuggy quartz associated with some ore and hydrothermal minerals in the area are typical of HS epithermal deposits such as enargite and alunite (Fig. 4a-c).

4.2. Image analysis for detecting hydrothermal alteration and lineament extraction

The first step in satellite image digital processing is the review of raw parameters of satellite images. Calculated statistical parameters of the raw satellite data have been presented in Table 1. Digital image processing should always be done after radiometric and geometric corrections. In this study, we used false color combination for indication of lithology for the study area. We applied different combinations of bands for the ETM+ 5 and ETM+ 7 Landsat images. 7, 4, 1 and 7, 5, 4 band combinations have been distinguished as the best combination for this area. Intrusions in the study area that host mineralization, and ore mineralization related to them, consist of one broad suite of early quartz monzonite to quartz syenite porphyry stock and an alkali granite porphyry stock. They are distinguishable and differentiated because of their felsic and intermediate composition and looking lighter in color.

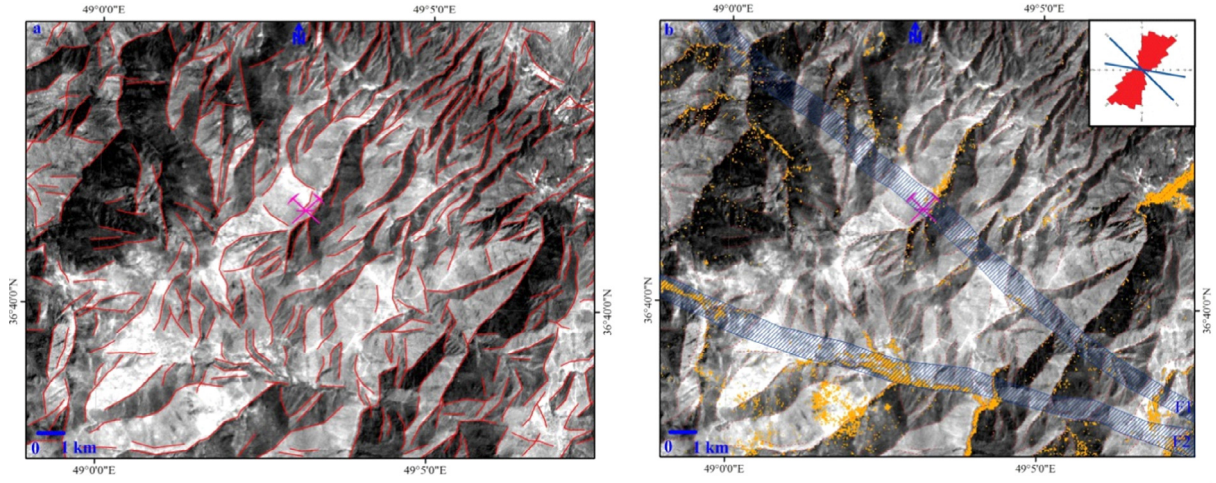

Fig. 6. a) Lineaments on processed PC1 image; b) argillic alteration, lineaments, two recognized fault zones and Chodarchay deposit in the processed PC1 image.

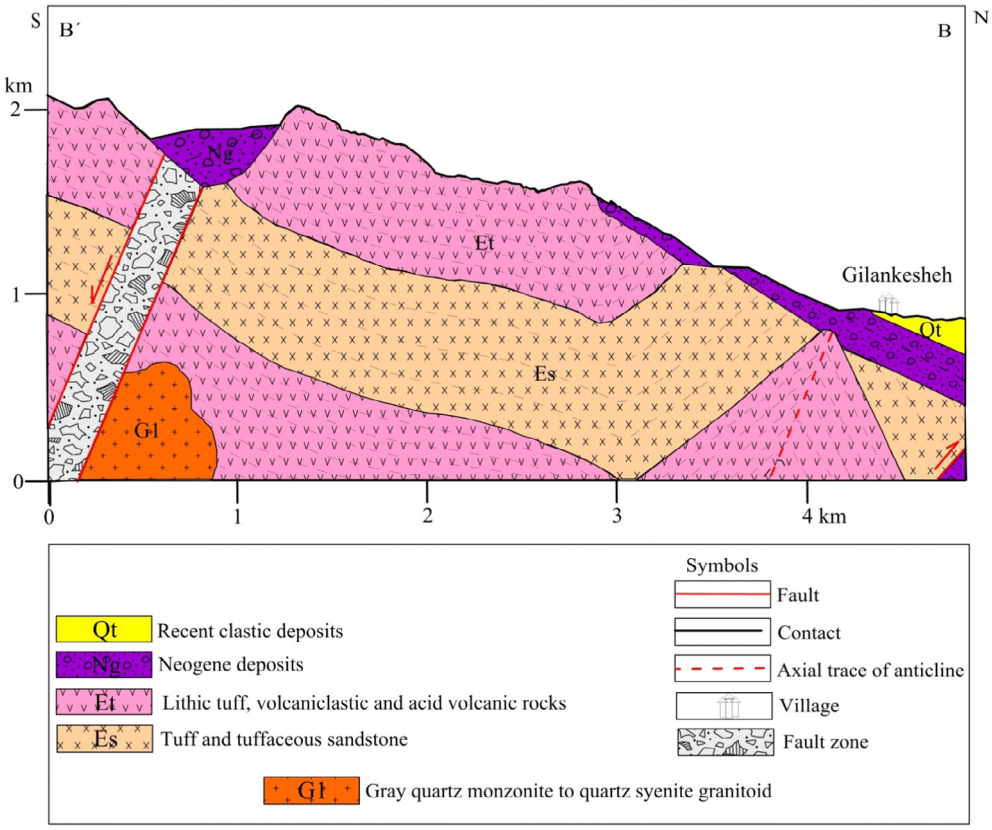

Fig. 7. Schematic section of the BB′ survey profile in the study area. Brecciated fault zone of the F1 Fault shows normal separation; however, structural data from the fault zone documents thrust kinematics for the fault.

In this study, for the indicated lithological specifications, in addition to false color combination, the Sultan Color Composite method has been used that includes 5/7, 5/1 and 5/4 * 3/4 band ratios in BGR, respectively (Sultan et al., 1986). Band ratios and multiplication techniques are sensitive to characteristic mineralogical and chemical constituents of the rocks to maximize rock discrimination. Consequently, composite ratio image of band 5/7, 5/1, and 5/4 * 3/4 set into R, G, B, respectively (Sultan's color), is a proportionate image suitable for individualizing lithological units. This technique displays felsic and granitic rocks in green–blue hues (Ali et al., 2012). In the studied image, felsic and intermediate granitic rocks are pale blue. The argillic alteration is orange to red. The red color of the argillic alteration is ascribed to the band 7 high absorption feature of hydroxyl-bearing minerals (Fig. 5a). In this study, after applying these methods to images, because of the high reflection of clay minerals in band 7 and their low reflection in band 5, we used 5/7 band ratio for determination of argillic alteration (Fig. 5b). The obtained DN values for each pixel in the altered rocks are about 100 (and darker). Values more than 145 (lighter) are usually used for argillic altered parts.

The principal component analysis method and the principal analysis component (PC1) image with the highest information were used for lineament extraction. The obtained image was processed by Geomatica 2015 and lineament extraction filters. Argillic alteration and lineaments were characterized on the processed image. From determination of lineaments on the map, two lineaments with a NW-SE trend were recognized. Field observation documents that the F1 and F2 lineaments are real fault zones and the

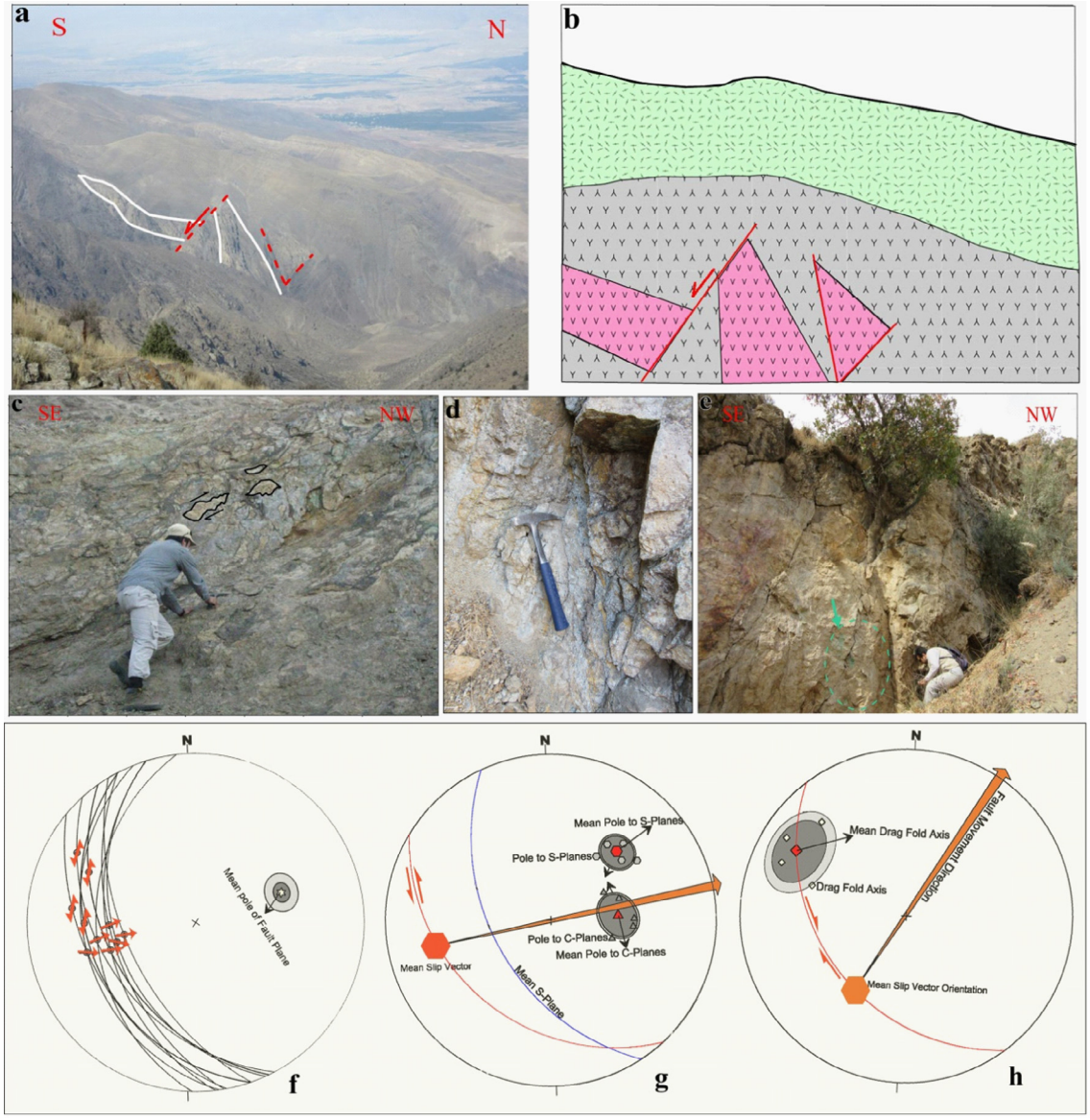

Fig. 8. Structural features from F1 Fault zone: a) normal displacement of the Eocene volcaniclastics in the F1 Fault zone. The F1 Fault was not completely inverted during the middle to late Miocene compressional event. b) Schematic line drawing of Fig. 8a. c) Fault zone of the F1 Fault that shows S-C fabric foliation with a thrust mechanism. d) Close-up view of Fig. 8c, S-C fabric foliation in the F1 fault zone. e) F1 Fault plane with slickensides. f) Stereographic projection of the slickenlines from the F1 Fault zone that generally indicates thrust with a right lateral strike-slip component kinematics. Several fault planes and related slickensides have been measured. The mean pole of the fault plane is shown by concentric circles on the stereographic projection. g) Stereographic projection of the S-C fabric foliation from the F1 Fault zone that generally has thrust with a right lateral strike-slip component kinematics. Several S and C planes have been measured and their mean poles presented as red hexagons in the figure. h) Stereographic projection of drag folds from F1 Fault zone that generally show the thrust kinematics. (For interpretation of the references to color in this figure legend, the reader is referred to the web version of this article.)

others are just topographic line features. We could not find any kind of topographic features including the offset and deflection of the river channels to prove these faults. However, structural field evidence represents deformation of the rock units along their fault zones. The Chodarchay deposit lies on one of these fault zones. Argillic alteration is observed to be dominant in the fault zones (Fig. 6 a-b).

4.3. Surface structural data set

Structural data have been gathered along a structural transect that cross-cuts the Tarom range in the Chodarchay mineralization site. The transect locations where the data have been gathered are presented on the Roudbar 1:100,000 geological map (Nazari and Salamati, 1998) (Fig. 2). The study area has been affected by two major fault zones, the F1 and F2 faults that control mineralization and its spatial distribution at the Chodarchay Cu-Au deposit. There is a major structural zone at the Chodarchay deposit that has similar strike to other regional faults in the area and the two major trends of Tarom intrusions. The trend of the F1 fault zone continues to the NW and SE beyond the Chodarchay deposit (Figs. 2 and 6b). The F1 Fault includes the main body of the ore deposit with a NW-SE trend and dipping SW. Core and damage zone related to the fault are approximately 100–150 m across. For better presentation of the structural geometry and kinematics of the region, two major cross sections have been drawn to explain the structures. The location of the cross sections has been presented on the geological map of the region (Fig. 2).

Cross section BB' is constructed at northwestern part of the Chodarchay deposit (Figs. 2 and 7). The separation along the fault which could be observed in the cross section represents normal movement. There is also some field evidence of normal faulting along

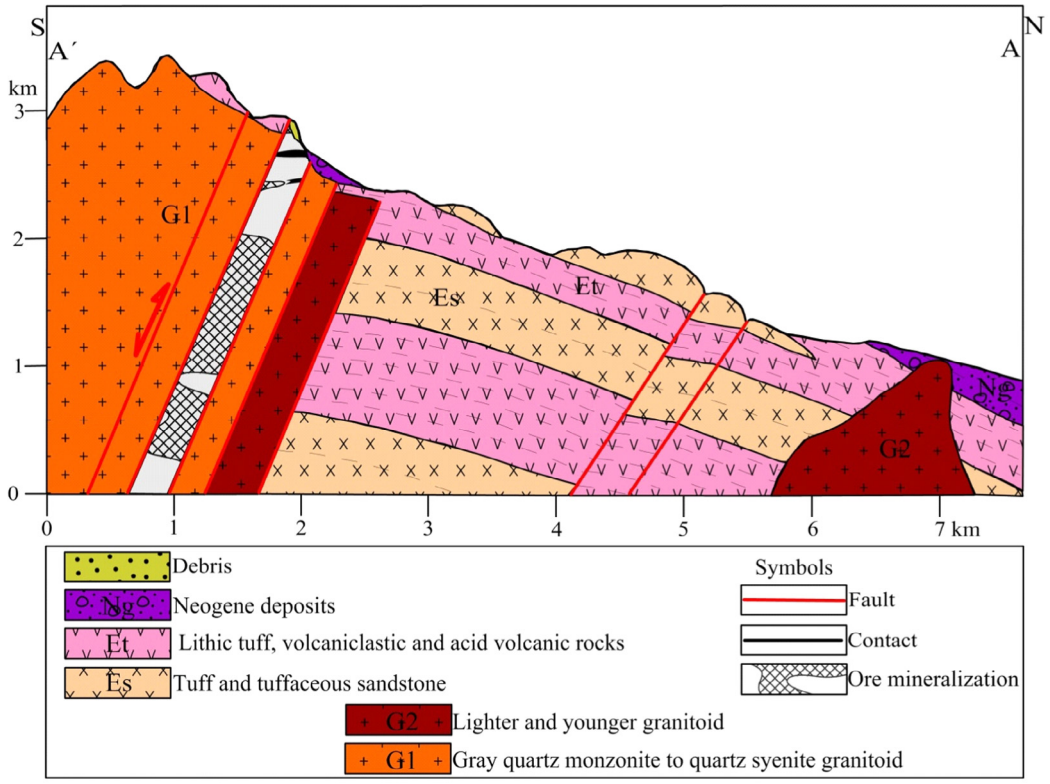

Fig. 9. Schematic section of the AA′ survey profile in the study area.

Fig. 10. Structural and sedimentological field evidence from the F1 Fault zone: a) folded veinlets in the F1 Fault zone. The folds axis has been used in kinematic analysis of the fault (see stereographic projection of Fig. 8g). b) F1 Fault surface and slickensides that has been used for the kinematic analysis given in the stereographic projection of Fig. 10e. c) Relics of the Paleogene – Neogene clastics and marls associated with the F1 Fault zone. This reflects a mini basin developed in the hanging-wall of the F1 Fault when it had normal offset during the early to late Oligocene.

the F1 Fault in which Eocene-lower Oligocene volcaniclastic rocks have normally been displaced (Fig. 8a-b). However, kinematic analysis of the fault zone structures in the area, including fault striations and S-C fabric foliations, shows thrust kinematics with a right lateral strike-slip component (Fig. 8c-e). The orientations of the sigmoidal shapes also show thrust kinematics for the fault (Fig. 8f-g). The veinlets developed in the fault zone of the F1 Fault also have a sigmoidal shape that is used for kinematic analysis. Eocene volcaniclastic and volcanic rocks are slightly folded in this section (Fig. 7). This fold is unconformably covered by Neogene clastics comprising mainly sandstone, conglomerate and marl. Cross section AA' is from southern part of Gilankesheh village into the Chodarchay ore deposit region (Fig. 9). There are two intrusive bodies in this section. The southern body, which hosted the porphyry and epithermal mineralization, is affected by F1 Fault. The fault is cut through the G1 intrusive body. The kinematic analysis of the F1 Fault in this section, using asymmetric drag folds (Fig. 10a) and slickensides on a fault surface (Fig. 10b), shows thrust kinematics (Fig. 8h). Relics of the Neogene deposits have also been observed in the fault zone of the F1 Fault (Figs. 7 and 10c).

4.4. Subsurface structural data set

For the study of preferred orientations of the joint and fracture systems in the Chodarchay deposit area, we also examined drill core. Fault-related fractures and faults filled with gouge material have been seen in the logged cores (Fig. 11a-f). Two dominant fracture orientations containing striations with reverse movement kinematics have been detected in the core logs (Fig. 11a-d).

In the diagram of dip angle of a fracture plotted against frequency, the 60° angle is dominant with a lesser peak at 40° in different fractures and the veinlets filled by quartz, carbonate and tourmaline (Fig. 12 a-d). Existence of these two dominant fractures in the cores, accords with two intersecting F1 and F2 fault fractures in field studies (Figs. 1b and 2). The dominant set of dipping faults in the drill cores has the same dip angle as fault F1. The graphs

Fig. 11. Samples of the cores and fault-related fractures in the Chodarchay ore deposit: (a, b) orientation and dip angle of the fractures in the cores of the Chodarchay deposit. Two sets of fractures with different orientations and fillings recorded in the cores. (c, d) outlined fracture zones. (e, f) slickensides and their movement directions documented on fracture planes.

indicate a correlation between fault fracture (N = 1204) dip angles and siliceous veinlets (N = 224) in the study area (Fig. 12a-b). This relationship is not as clear for tourmaline (N = 84) and calcite (N = 39) veinlets because of their lower frequency (Fig. 12c-d). All the surface and subsurface data sets show the structural control of the F1 fault zone in emplacement and later deformation of the Chodarchay ore deposit.

5. Discussion

5.1. Porphyry and epithermal mineralization in the Chodarchay deposit area

Several studies such as those of Arribas (1995) and Hedenquist et al. (1998) have documented genetic relationships between porphyry and HS type epithermal mineralization. However, there are still many unanswered questions regarding some porphyry and HS deposit couplets being spatially separated, while others are overprinted.

The Chodarchay deposit is an HS epithermal copper deposit with a sub-economic porphyry mineralization component. It offers an opportunity to assess structural controls on these two mineralization systems. The ore body is parallel to and emplaced within the F1 fault zone. The Chodarchay deposit lies within a wide fault zone (50–100 m) with ~ 60° dip angle and a NW–SE trend, so that the term mineralization zone could be appropriate. The granitoid stock is emplaced and hydrothermal fluids flow within local strain features of the F1 fault system, including calcite, quartz and tourmaline veinlets. Cross-cutting relations observed in the field show that the HS epithermal part formed after emplacement of the porphyry stock and associated mineralization. This overprinting occurred due to reverse-sense reactivation of an initially normal F1 fault during exhumation of the granitoid stock. The epithermal part of the Chodarchay deposit is hosted by the volcanic and pyroclastic rocks of the Karaj Formation and the cross-cutting post Eocene plutonic intrusions. The plutonic intrusions include quartz monzonite and granite units that host the porphyry mineralization part of the deposit. The epithermal part of the deposit is characterized by multiphase brecciation and opening and therefore multistage ore deposition. The ore body forms massive silicified breccia, stockwork zones and disseminations usually found along the F1 fault system structures. Epithermal mineralization in some parts of the deposit shows an association with a steeply dipping reverse fault on the granitoid intrusive footwall rocks.

5.2. Structural control of ore mineralization in the Chodarchay deposit area

Spatial and temporal relations between ore mineralization and major intercontinental fault zones have been reported by some researchers in various mineralized districts around the world (e.g., Gow and Walshe, 2005). However, the relationships between intrusion-related mineralization and brittle structures are not statistically robust, and have been suggested to be caused by subjective bias (Paterson and Schmidt, 1999). Most porphyry copper deposits are generally considered to have formed during the later stages of compressional deformation through to incipient extension in magmatic arcs above subduction zones (e.g., Gow and Walshe, 2005; Heidrick and Titley, 1982; Tosdal and Richards, 2001). Partly due to scale-dependencies that are rarely considered, there are conflicting hypotheses about the relative importance of contractional, extensional and strike-slip strain accommodation during porphyry emplacement.

Incompatible models have proposed the great effect of strike-slip and reverse faulting during emplacement of porphyry and epithermal systems (Cooke et al., 2005). Based on regional studies, the structural data set including analysis of satellite images (Figs. 5 and 6), field-based structural analysis (cross sections A-A′ and B-B′) and subsurface drill core analysis, show that a major fault zone controls spatial and temporal distribution of the Chodarchay ore deposit. Figs. 7 and 9 give cross sections based on the field data. Kinematic data from the F1 Fault zone show thrust with right lateral strike slip kinematics (Fig. 8f-h). However, cross sections show a normal stratigraphic separation on the F1 Fault (Figs. 7 and 9). This would suggest an earlier normal kinematics of the F1 fault

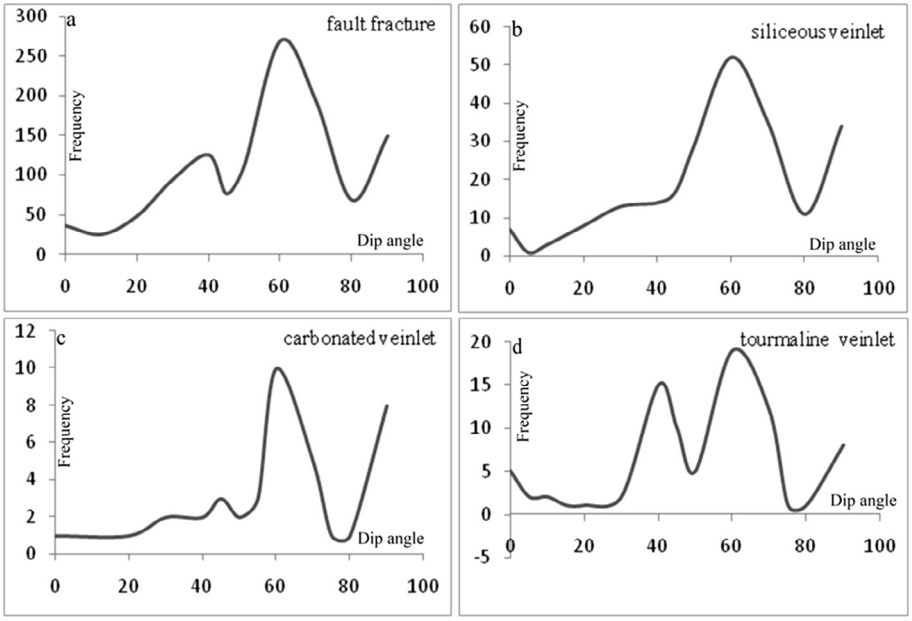

Fig. 12. Diagrams show the frequency of the different dip angle of fractures measured in cores from the Chodarchay deposit: a) a total of 1204 fractures measured in the core logging data. b) Frequency of the dip angle of the 204 veinlets filled with siliceous materials. c) Frequency of the dip angle of the 39 veinlets filled with carbonate materials. d) Frequency of the dip angle of the 84 veinlets filled with tourmaline materials.

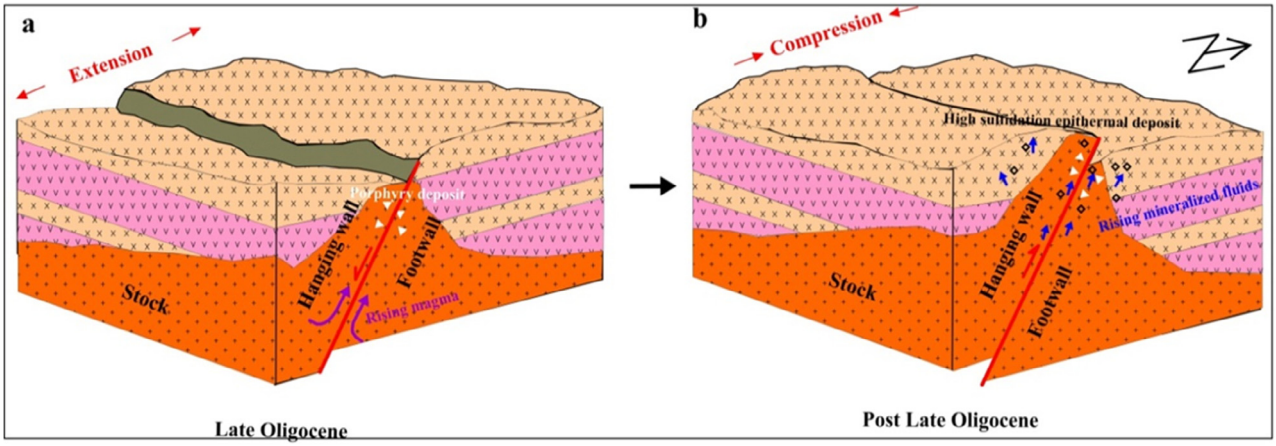

Fig. 13. Block diagrams showing structural and mineralization evolution of the Chodarchay deposit in the Tarom subzone of the Alborz magmatic belt. a) Eocene to late Oligocene extensional related porphyry mineralization of the Chodarchay deposit. b) Regional kinematic change at the Alborz magmatic belt from extension to compression due to Arabia and Eurasia continental collision in the middle Miocene. High-sulfidation epithermal deposit has overprinted porphyry mineralization at this time.

during the Eocene – early Oligocene that had not been fully reactivated by thrusting during the middle Miocene compressional event of the Alborz magmatic belt. However, the fault striations from the eastern segment of the fault have a reverse with a right lateral strike-slip component that postdates and overprints normal shear sense indicators. Two sets of fault fractures led to the formation of fault lenses (Fig. 8c). In the mineralized zone, signs of mineralization could be seen on the reverse fault wall (Fig. 8e) and there are some quartz veins in the host rocks. This proves that for the Chodarchay deposit, HS Cu-Au mineralization was superimposed into the porphyry part along the reverse faults.

The structural field data set combined with geodynamic models proposed for the NW Iranian Plateau tectonic evolution (Madanipour et al., 2013), represent a major reorganization from late Eocene – early Oligocene extension to late Oligocene – middle Miocene compression around the Chodarchay mineralization site (Fig. 13a-b). These deformation and magmatism events have also been reported for other parts of the Alborz magmatic belt, especially in the Tarom subzone (e.g., Castro et al., 2013; Nabatian et al., 2016). High-sulfidation epithermal mineralization formed during inversion of the major fault from normal to reverse mechanism when the extensional tectonic regime was in transition to a compressional one during the early Oligocene to early Miocene (Fig. 13b).

6. Conclusions

Recognition of alteration and lineaments in processed satellite imagery established that NW-trending fractures controlled the Chodarchay deposit. The structural data set, including field and subsurface core drillings, proved that this lineament is a fault zone. Therefore, Chodarchay mineralization and the fault zone are related to each other. One main fault zone with both normal and reverse mechanisms during its late Cenozoic evolution was identified in the Chodarchay area. The fault cross-cuts the Chodarchay deposit area. Field observations show that this fault zone, that cross-cut the rock units in Chodarchay, was active during the hydrothermal episodes. These structures likely acted as conduits for the epithermal mineralizing fluids. Potassic alteration (K-feldspar + biotite + magnetite) and associated chalcopyrite mineralization indicate a linkage with an underlying porphyry copper deposit. During this mineralization event, the fault was kinematically normal. Based on field evidence and drill core studies, it appears that the porphyry part is related to first and normal stage and the epithermal part is associated with the second inversion stage of the main fault. The deposit was overprinted by high-sulfidation epithermal type during the compressional stage. Coexistence of these two types of mineralization controlled by structural elements is reported for the first time in the Tarom subzone.

Acknowledgements

This paper is part of the first author's Ph.D. thesis project. Financial support was provided by Tarbiat Modares University of Iran. Appreciation is extended to Madankaran Angouran Company for generously providing field survey facilities and access to drill cores and exploration data. We would like to thank Chris Fergusson and Abbas Babaahmadi for their constructive reviews on the manuscript. Franco Pirajno and Hooshang Asadi Haroni are also thanked for careful editorial handling of the manuscript.

References

Agard, P., Omrani, J., Jolivet, L., Mouthereau, F., 2005. Convergence history across Zagros (Iran): constraints from collisional and earlier deformation. Int. J. Earth Sci. 94, 401–419.

Aghazadeh, M., Castro, A., Badrzadeh, Z., Vogt, K., 2011. Post-collisional polycyclic plutonism from the Zagros hinterland: the Shaivar Dagh plutonic complex, Alborz belt. Iran. Geol. Mag. 148, 980–1008.

Ahmadian, J., Haschke, M., McDonald, I., Regelous, M., Ghorbani, M.R., Emami, M.H., Murata, M., 2009. High magmatic flux during Alpine-Himalayan collision: constraints from the Kal-e-Kafi complex, central Iran. Geol. Soc. Am. Bull. 121, 857–868.

Ali, E.A., Khidir, S.O.E., Babikir, I.A.A., Abdelrahman, E.M., 2012. Landsat ETM+7 digital image processing techniques for lithological and structural lineament enhancement: case study around Abidiya area, Sudan. Open Remote Sens. J. 5, 83–89.

Allen, M.B., Armstrong, H.A., 2008. Arabia-Eurasia collision and the forcing of mid-Cenozoic global cooling. Palaeogeogr., Palaeocl. 265, 52–58.

Allen, M.B., Ghassemi, M.R., Shahrabi, M., Qorashi, M., 2003. Accommodation of late Cenozoic oblique shortening in the Alborz range, northern Iran. J. Struct. Geol. 25, 659–672.

Allen, M., Jackson, J., Walker, R., 2004. Late Cenozoic reorganization of the Arabian-Eurasian collision and the comparison of short-term and long-term deformation rates. Tectonics 23.

Amidi, S.M., Emami, M.H., Michel, R., 1984. Alkaline character of Eocene volcanism in the middle part of Iran and its geodynamic situation. Geol. Rundsch. 73, 917–932.

Arian, M., Nouri, R., 2015. Lineament tectonics and mineralization in Tarom area, north Iran. Open J. Geol. 5, 115–125. http://dx.doi.org/10.4236/ojg.2015.53011.

Arribas Jr., A., 1995. Characteristics of high-sulfidation epithermal deposits, and their relation to magmatic fluid. Mineral. Assoc. Canada Short Course 23, 419–454.

Asiabanha, A., Foden, J., 2012. Post-collisional transition from an extensional volcanosedimentary basin to a continental arc in the Alborz Ranges, N-Iran. Lithos 148, 98–111. http://dx.doi.org/10.1016/j.lithos.2012.05.014.

Azizi, H., Tanaka, T., Asahara, Y., Chung, S.L., Zarrinkoub, M.H., 2011. Discrimination of the age and tectonic setting for magmatic rocks along the Zagros thrust zone,

north-west Iran, using the zircon U-Pb age and Sr–Nd isotopes. J. Geodyn. 52, 304–320.
Ballato, P., Uba, C.E., Landgraf, A., Strecker, M.R., Sudo, M., Stockli, D.F., Friedrich, A., Tabatabaei, S.H., 2011. Arabia-Eurasia continental collision: insights from late Tertiary foreland-basin evolution in the Alborz Mountains, Northern Iran. Bull. Geol. Soc. Am. 123 (1–2), 106–131. http://dx.doi.org/10.1130/B30091.1.
Berberian, M., 1983. The southern Caspian: a compressional depression floored by a trapped, modified oceanic crust. Can. J. Earth Sci. 20, 163–183.
Berberian, F. and Berberian, M., 1981. Tectono-plutonic episodes in Iran. In: Gupta, H.K., Delany, F.M. (eds.), Zagros. Hindu Kush, Himalaya Geodynamic Evolution. Geodyn. Ser. 3. American Geophysical Union, Washington, DC, 5–32.
Berberian, M., King, G.C., 1981. Toward a paleogeography and tectonic evolution of Iran. Can. J. Earth Sci. 18, 210–265.
Berberian, F., Muir, I.D., Pankhurst, R.J., Berberian, M., 1982. Late Cretaceous and early Miocene Andean type plutonic activity in northern Makran and central Iran. J. Geol. Soc. Lond. 139, 605–614.
Berger, B.R., Drew, L.J., 1997. Role of strike-slip duplexes in localization of volcanoes, related intrusions, and epizonal ore deposits [abs.]. Geol. Soc. Am. Abstracts with Programs 29 (6), A359–A360.
Berger, B.R., Drew, L.J., Singer, D.A., 1999. Quantifying mineral-deposit models for resource assessment. Geol. Hung. 24, 41–54.
Carranza, E.J.M., Hale, M., 2002. Where are porphyry copper deposits spatially localized? A case study in Benguet Province, Philippines. Nat. Resour. Res. 11 (1), 45–59.
Castro, A., Aghazadeh, M., Badrzadeh, Z., Chirro, M., 2013. Late Eocene-Oligocene post-collisional monzonitic intrusions from the Alborz magmatic belt, NW Iran. An example of monzonite magma generation from a metasomatized mantle source. Lithos 180, 109–127. http://dx.doi.org/10.1016/j.lithos.2013.08.003.
Cooke, D.R., Hollings, P., Walshe, J.L., 2005. Giant porphyry deposits – characteristics, distribution and tectonic controls. Econ. Geol. 100, 801–818.
Drew, L.J., Berger, B.R., 2001. Model of the porphyry copper/polymetallic vein kin-deposit system; Application in the Metaliferi Mountains, Romania. In: Piestrzyński, Adam. (Ed.), Mineral Deposits at the Beginning of the 21st Century: Exton, Penn. A.A. Balkema Press, Exton, Penn., pp. 519–522.
Drew, L.J., Berger, B.R., 2002. Application of the porphyry copper/polymetallic vein kin deposit system to mineral-resource assessment in the Mátra Mountains, northern Hungary. In: Fabbri, A.G., Gaál, Gabor, McCammon, R.B. (Eds.), Deposit and geoenvironmental models for resource exploitation and environmental security. Kluwer Acad. Publ., Boston, pp. 171–186.
Drew, L.J., Berger, B.R., Bawiec, W.J., Sutphin, D.M., Csirik, G., Korpás, L., Vetö-Akos, E., Odor, L., Kiss, J., 1999a. Mineral-resource assessment of the Mátra and Börzsöny-Visegrád Mountains, north Hungary. Geol. Hung. 24, 79–96.
Drew, L.J., Singer, D.A., Menzie, W.D., Berger, B.R., 1999b. Mineral-resource assessment—state of the art. Geol. Hung. 24, 31–40.
Fakhari, M.D., Axen, G.J., Horton, B.K., Hassanzadeh, J., Amini, A., 2008. Revised age of proximal deposits in the Zagros foreland basin and implications for Cenozoic evolution of the High Zagros. Tectonophysics 451, 170–185.
Ghasemi, A., Talbot, C.J., 2006. A new tectonic scenario from the Sanandaj-Sirjan Zone (Iran). J. Asian Earth Sci. 26, 683–693.
Gow, P.A., Walshe, J., 2005. The role of preexisting geologic architecture in the formation of giant porphyry-related Cu Au deposits: Examples from New Guinea and Chile. Economic Geology 100th Anniversary Volume.
Guest, B., Horton, B.K., Axen, G.J., Hassanzadeh, J., McIntosh, W.C., 2007. Middle to late Cenozoic basin evolution in the western Alborz Mountains: implications for the onset of collisional deformation in northern Iran. Tectonics 26.
Haschke, M., Ahmadian, J., Murata, M., Mcdonald, I., 2010. Copper mineralization prevented by arc–root delamination during Alpine-Himalayan collision central Iran. Econ. Geol. 105, 855–865.
Hassanzadeh, J., 1993. Metallogenic and tectono-magmatic events in the SE sector of the Cenozoic active continental margin of Iran (Shahr e Babak area, Kerman province) (Unpublished Ph.D. thesis). University of California, Los Angeles. 204 p..
Hassanzadeh, J., Ghazi, A.M., Axen, G., Guest, B., 2002. Oligo-Miocene mafic alkaline magmatism north and northwest of Iran: Evidence for the separation of the Alborz from the Urumieh-Dokhtar magmatic arc. Geol. Soc. Am. Abstracts with Programs 34, 331.
Hedenquist, J.W., Arribas Jr, A., Reynolds, T.J., 1998. Evolution of an intrusion centered hydrothermal system: Far Southeast-Lepanto porphyry and epithermal Cu-Au deposits, Philippines. Econ. Geol. 93, 373–409.
Heidrick, T.L., Titley, S.R., 1982. Fracture and dike patterns in Laramide plutons and their structural and tectonic implications. In: Titley, S.R. (Ed.), Advances in Geology of Porphyry Copper Deposits of Southwestern North America. U. Ariz. Press, Tuscon, pp. 73–91.
Heuret, A., Lallemand, S., 2005. Plate motions, slab dynamics and back-arc deformation. Phys. Earth Planet. Inter. 149 (1–2), 31–51. http://dx.doi.org/10.1016/j.pepi.2004.08.022.
Heuret, A., Funiciello, F., Faccenna, C., Lallemand, S., 2007. Plate kinematics, slab shape and back-arc stress: A comparison between laboratory models and current subduction zones. Earth Planet. Sc. Lett. 256 (3–4), 473–483. http://dx.doi.org/10.1016/j.epsl.2007.02.004.
Hirayama, K., Samimi, M., Zahedi, M., Hushmand-zadeh, A., 1966. Geology of Taroum district, western part (Zanjan area north-west Iran). Geol. Surv. Iran.
Honarmand, M., Rashidnejad Omran, N., Neubauer, N., Emami, M.H., Nabatian, G., Liu, X., Donge, Y., von Quadt, A., Chen, B., 2013. Laser-ICP–MS U-Pb zircon ages and geochemical and Sr–Nd–Pb isotopic compositions of the Niyasar plutonic complex, Iran: constraints on petrogenesis and tectonic evolution. Int. Geol. Rev. 56, 104–132.
Horton, B.K., Hassanzadeh, J., Stockli, D.F., Axen, G.J., Gillis, R.J., Guest, B., Amini, A., Fakhari, M.D., Zamanzadeh, S.M., Grove, M., 2008. Detrital zircon provenance of Neoproterozoic to Cenozoic deposits in Iran: Implications for chronostratigraphy and collisional tectonics. Tectonophysics 451, 97–122.
Jackson, J., Priestley, K., Allen, M., Berberian, M., 2002. Active tectonics of the south Caspian Basin. Geophys. J. Int. 148, 214–245.
Jahangiri, H., 2007. Post-collisional Miocene adakitic volcanism in NW Iran: geochemical and geodynamic implications. J. Asian Earth Sci. 30, 433–447.
Janković, S., 1977. The copper deposits and geotectonic setting of the Tethyan Eurasian metallogenic belt. Mineral. Deposita 12 (1), 37–47.
Karsli, O., Chen, B., Aydin, F., Şen, C., 2007. Geochemical and Sr–Nd–Pb isotopic compositions of the Eocene Dölek and Sariçiçek Plutons, Eastern Turkey: implications for magma interaction in the genesis of high-K calc-alkaline granitoids in a postcollision extensional setting. Lithos 98, 67–96. http://dx.doi.org/10.1016/j.lithos.2007.03.005.
Madanipour, S., Ehlers, T.A., Yassaghi, A., Rezaeian, M., Enkelmann, E., Bahroudi, A., 2013. Synchrounous deformation on orogenic plateau margins, insights from the Arabia-Eurasia collision. Tectonophysics 608, 440–451. http://dx.doi.org/10.1016/j.tecto.2013.09.003.
Mirnejad, H., Hassanzadeh, J., Cousens, B.L., Taylor, B.E., 2010. Geochemical evidence for deep mantle melting and lithospheric delamination as the origin of the inland Damavand volcanic rocks of northern Iran. J. Volcanol. Geoth. Res. 198 (3–4), 288–296. http://dx.doi.org/10.1016/j.jvolgeores.2010.09.014.
Moayyed, M., 2001. Geochemistry and petrology of volcano-plutonic bodies in Tarom area (Ph.D. thesis). University of Tabriz, Iran (256 pp. in Persian with English abstract).
Moinvaziri, H., 1985. Volcanism etertiaire etquaternaire en ba These d'Etat Université Paris-Sud, Orsay, pp. 278.
Nabatian, G., Ghaderi, M., Neubauer, F., Honarmand, M., Lui, X., Dong, Y., Jiang, S.-Y., Bernroider, M., 2014. Petrogenesis of Tarom high-potassic granitoids in the Alborz–Azarbaijan belt, Iran: geochemical, U-Pb zircon and Sr–Nd–Pb isotopic constraints. Lithos 184–187, 324–345. http://dx.doi.org/10.1016/j.lithos.2013.11.002.
Nabatian, G., Giang, S.Y., Honarmand, M., Neubauer, F., 2016. Zircon U-Pb ages, geochemical and Sr-Nd-Pb-Hf isotopic constraints on petrogenesis of the Tarom-Olya pluton, Alborz magmatic belt. Lithos 244, 43–58. http://dx.doi.org/10.1016/j.lithos.2015.11.020.
Nazari, H., Salamati, R., 1998. Roudbar 1:100,000 Geological map.
Nouri, R., Jafari, M.R., Arian, M., Feizi, F., Afzal, P., 2013. Correlation between Cu mineralization and major faults using multifractal modelling in the Tarom area (NW Iran). Geol. Carpath. 64, 409–416. http://dx.doi.org/10.2478/geoca-2013-0028.
Agard, P., Omrani, J., Jolivet, L., Whitechurch, H., Vrielynck, B., Spakman, W., Monié, P., Meyer, B., Wortel, R., 2011. Zagros orogeny: a subduction-dominated process. Geol. Mag. 148, 692–725.
Paterson, S.R., Schmidt, K., 1999. Is there a close spatial relationship between faults and plutons? J. Struct. Geol. 21. 1131-114.
Richards, J.P., 2005. Cumulative factors in the generation of giant calc-alkaline porphyry Cu deposits. In: Porter, T.M. (Ed.), Super porphyry copper and gold deposits: a global perspective, v. 1. PGC Publishing, Adelaide, pp. 7–25.
Richards, J.A., Xiuping, J., 2006. Remote Sensing Digital Image Analysis: An Introduction. Springer, Germany.
Stöcklin, J., 1971. Stratigraphic Lexicon of Iran; Part 1. Geological Survey of Iran, Tehran, Iran, 338 p.
Stöcklin, J., 1974. Possible ancient continental margins in Iran. In: Burk, C.A., Drake, C.L. (Eds.), The Geology of Continental Margins. Springer, Berlin, pp. 873–887.
Sultan, M., Arvidson, R.E., Sturchio, N.C., 1986. Mapping of serpentinites in the Eastern Desert of Egypt by using landsat thematic mapper data. Geology 14, 995–999.
Taylor, B., Martinez, F., 2003. Back-arc basin basalt systematics. Earth Planet. Sci. Lett. 210 (3–4), 481–497. http://dx.doi.org/10.1016/S0012-821X(03)00167-5.
Tosdal, R.M., Richards, J.P., 2001. Magmatic and structural controls on the development of porphyry Cu ± Mo ± Au deposits. Rev. Econ. Geol. 14, 157–181 http://dx.doi.org/doi:10.5382/Rev.14.06.
Uyeda, S., 1982. Subduction zones: An introduction to comparative subductology. Tectonophysics 81 (3–4), 133–159. http://dx.doi.org/10.1016/0040-1951(82)90126-3.
Verdel, C., Wernicke, B.P., Hassanzadeh, J., Guest, B., 2011. A Paleogene extensional arc flare-up in Iran. Tectonics 30, TC3008. http://dx.doi.org/10.1029/2010TC002809.
Vernant, P., Nilforoushan, F., Hatzfeld, D., Abbassi, M.R., Vigny, C., Masson, F., Nankali, H., Martinod, J., Ashtiani, A., Bayer, R., Tavakoli, F., Chéry, J., 2004. Present-day crustal deformation and plate kinematics in the Middle East constrained by GPS measurements in Iran and northern Oman. Geophys. J. Int. 157, 381–398.
Vincent, I., Allen, M.B., Ismail-Zadeh, A.D., Flecker, R., Foland, K.A., Simmons, D., 2005. Insights from the Talysh of Azerbaijan into the Paleogene evolution of the South Caspian region. Geol. Soc. Am. Bull. 117, 1513–1533.
Vincent, S.J., Morton, A.C., Carter, A., Gibbs, S., Barabadze, T.G., 2007. Oligocene uplift of the western Greater Caucasus: an effect of initial Arabia-Eurasia collision. Terra Nova 19, 160–166.